SEMARAK ILMU PUBLISHING

CFD Letters

Journal homepage:
https://semarakilmu.com.my/journals/index.php/CFD_Letters/index
ISSN: 2180-1363

Numerical Investigation of Hydrodynamics in Inline Mixers

Maulana Gilar Nugraha[1,*], Daffa Dewa Saputra[1], Khairullah Ilyas[1], Muslikhin Hidayat[1]

[1] Department of Chemical Engineering, Universitas Gadjah Mada, Jl. Grafika No.2, Yogyakarta 55281, Indonesia

ARTICLE INFO

Article history:
Received 17 February 2023
Received in revised form 16 March 2023
Accepted 14 April 2023
Available online 1 August 2023

Keywords:
Hydrodynamics; inline mixer; T-mixer; Y-mixer; elbow mixer; internal injection; wall shear stress; CFD

ABSTRACT

The utilization of inline mixers for continuous fluid mixing is a common practice in chemical industries. Information related to hydrodynamics condition in inline mixers is found to be limited while it is crucial for inline mixer type selection. Evaluation of hydrodynamic characteristics in several commercial inline mixers is analyzed in this study, including Y-type, T-type, elbow type, and internal injection mixer types. The analysis is conducted using computational fluid dynamics (CFD) for various Reynolds number conditions from 5,000 to 200,000. Mesh independence tests and model validation with experimental results are performed to ensure simulation accuracy. The CFD results showed that the Y-type mixer type provides the shortest distance i.e., about 12 times diameter. The internal injection type mixer has the most extended hydrodynamic region length to reach a fully-developed region for the same Reynolds number. The highest wall stress is indicated by the injection inline mixer type that located at the outer side wall of the injection pipe. The wall stress at that region is observed to be around twice as large compared to the other mixer type. Meanwhile, the mixer joint in the T-type and Y-type mixers were found to have a wall stress hotspot. Logarithmic correlation formulas were successfully formulated to correlate hydrodynamic region length and Reynolds number for all mixer types. The study results are essential in serving as the basis for inline mixer selection in the industrial sector.

1. Introduction

The mixing process, which includes solid, fluid, and gas phases, is a common process in the chemical industry. The process may occur either at the beginning, when different raw materials are mixed, or at the latest stage, where product purification takes place [1-2]. Several parameters must be considered in designing a fluid mixing process, e.g., operation mode (batch or continuous), fluid viscosity, and correlation of mixing to other physical phenomena such as reactive mixing and heat transfer. For relatively low-viscosity fluid mixing, which operates in continuous mode, inline mixers are frequently used in many chemical plants [3]. Several commercial inline mixers which are widely used include spatial-shaped mixers, such as Y-mixers and T-mixers, and injection mixers, such as internal and external injection mixers, as presented in Figure 1.

* *Corresponding author.*
E-mail address: maulana.gilar.n@mail.ugm.ac.id (Maulana Gilar Nugraha)

https://doi.org/10.37934/cfdl.15.8.135147

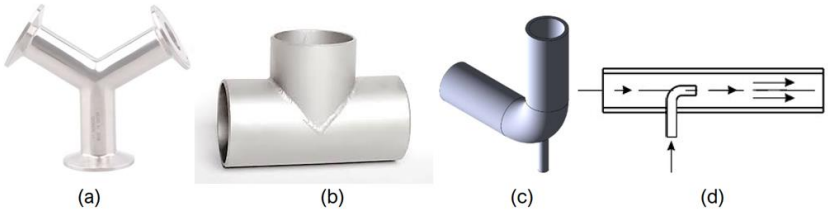

Fig. 1. Commercial inline mixer (a) Y-type, (b) T-type, (c) external injection, and (d) internal injection [3].

The mixing point of two or more streams in inline mixers might produce flow instability, usually referred to as the hydrodynamic region. The mixed stream will flow to the pipe downstream while the velocity profile gradually develops to be more stable and is usually referred to as a fully-developed region [4]. Information related to hydrodynamic parameters is considered to be crucial, especially for sensor placement in a pipe flow, including mass flow rate, pressure, temperature, and concentration sensors. Therefore, instead of measurement at a hydrodynamic region, observation at a fully-developed region is necessary to ensure measurement accuracy and stability. In addition, the availability of hydrodynamic properties is proven to be beneficial in obtaining piping stress distribution [5] and predicting the flow-accelerated corrosion region [6].

Numerous studies have been conducted to investigate hydrodynamics and mixing characteristics of inline mixers, especially T-type inline mixers, using experimental approaches [7–11]. Utilization of CFD analysis has been proven to improve the understanding of hydrodynamics and mixing phenomena happening inside inline mixers as presented by several previous studies [7, 8, 12–17]. Based on those works, it can be concluded that different flow parameters influence the hydrodynamic condition in inline mixers, including the angle between the branch and main pipe, diameter ratio, velocity ratio, and mass flow rate.

A comprehensive review related to mixing characteristics and the length of the hydrodynamic region in various inline mixers have not been presented in previous studies. An estimated range of hydrodynamic region length for different inline mixers was presented by Sinnot *et al.,* [3]. A length of pipe equal to 10 to 20 pipe diameters is required to provide satisfactory mixing in T-type inline mixers. On the other hand, internal mixers need approximately 80 pipe diameters to ensure a satisfactory blend. A better prediction of the length of hydrodynamic properties is crucial to optimize pipe dimension and piping layout in many industries. Moreover, hydrodynamic properties could also provide information related to pumping power necessity.

Based on the aforementioned challenges and research gaps, this study aimed to investigate the flow characteristics in the hydrodynamic region in various commercial inline mixers using numerical analysis in computational fluid dynamics (CFD) framework. The apparent significance of this study lies to determining the mixing length of each type of mixers in a way that guides picking a suitable inline mixer in industrial sector. Validation with an experimental investigation was also presented to ensure the accuracy of present comparisons. The influence of Reynolds number adjustment to the length of hydrodynamic region was examined to provide better overview of various range of flow conditions. This comprehensive comparison is essential as a basis for inline mixer selection and detail engineering design in industrial sector.

2. Methodology

This study analyzed the mixing performances of four different inline mixer types, consisting of two simple spatial-shaped mixers (Y-mixer and T-mixer) and two injection mixers (external injection

and internal injection mixers), through computational fluid dynamics (CFD) simulation. The simulation was carried out using ANSYS FLUENT 2022R1 software. Mixing performance was observed by measuring each inline mixer's hydrodynamic region length at varying Reynold numbers. The length of the hydrodynamic region of each mixer was obtained by monitoring the velocity fluctuations in the center of each mixing pipe. The results were subsequently compared to provide an overview of each mixer's performance. A representative result was then compared to the experimental study to validate the simulation model.

2.1 Geometry and Meshing

The geometrical details of each inline mixer are shown in Figure 2. The spatial-shaped mixers (Y-mixer and T-mixer) of the same inlet diameter were selected. Both mixers have inlet diameters of 2 inches (0.0508 meters) and a pipe angle of 90°. Alternately, the injection mixers have differing inlet diameters, with the main pipe having a diameter of 2 inches (0.0508 meters) and the injection pipe of 0,25 inches (0.0127 meters). Each injection point was determined at the center of the main pipe (0.5 D_1). In addition, a mixing pipe of 60 inches (1.524 meters) in length was used to measure every mixer's mixing length. All mixers were positioned horizontally so that gravitational influence could be neglected.

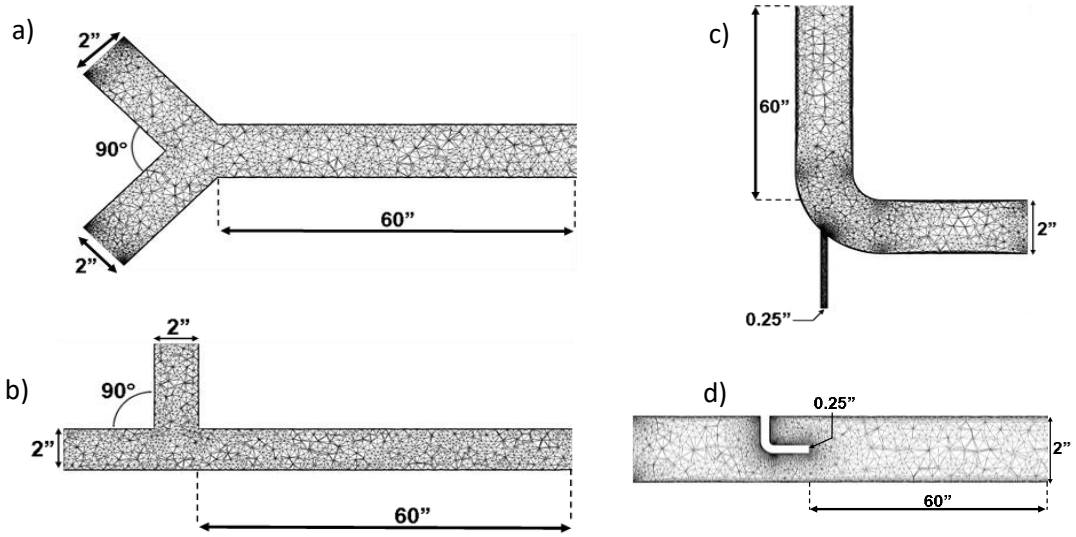

Fig. 2. Computational domain and final mesh for a) Y-Mixer, b) T-Mixer, c) External Injection (Elbow) Mixer, and d) Internal Injection Mixer

The computational domain was then discretized into computational cells using the mesh generator in ANSYS 2022R1. A mesh independence test was carried out beforehand to determine the number of elements needed to represent each mixer accurately. Each geometry was first meshed using hexahedral-shaped elements uniformly throughout the whole model. Subsequently, using a parametric analysis tool, the mesh was gradually increased based on y+ wall value and velocity gradient parameter. Intensive refinements were obtained at the near-wall region to provide average y^+ wall value of less than 3. The average velocity on various planes along the mixing pipe was monitored at different numbers of cells and is depicted in Figure 3. The final mesh that was utilized in the current work for different inline mixer type is summarized in Table 1.

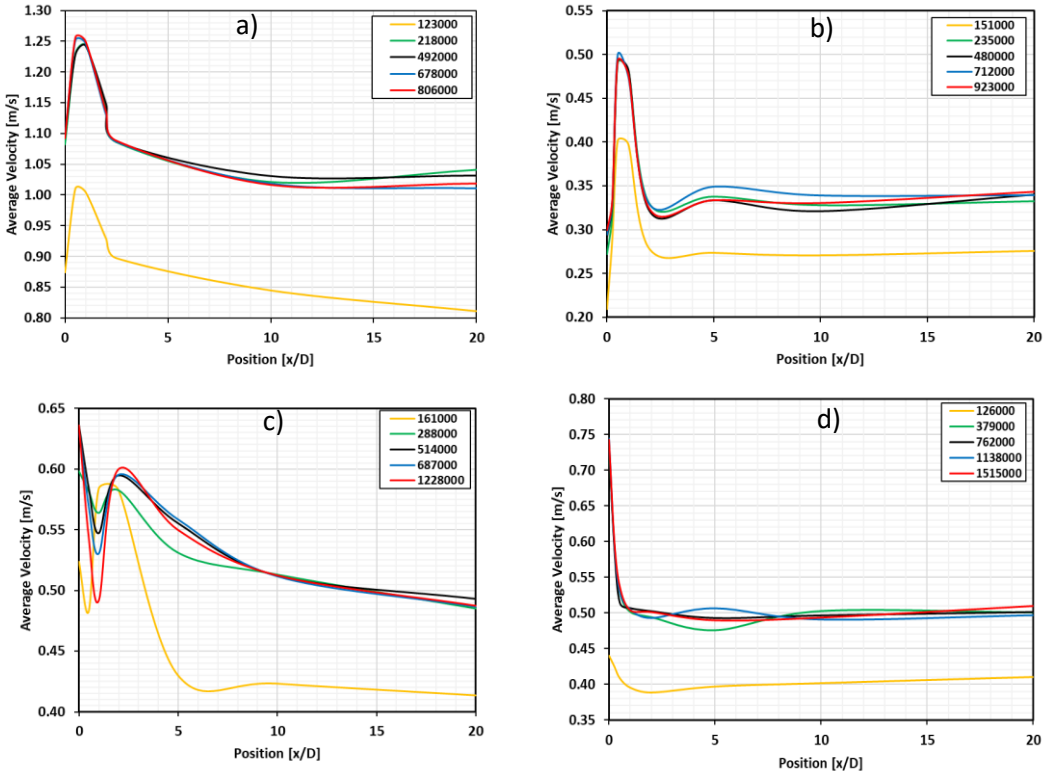

Fig. 3. Mesh independence test convergence graph on a) Y-Mixer, b) T-Mixer, c) External Injection (Elbow) Mixer, and d) Internal Injection Mixer

Table 1
Mesh independence test results

Parameters	Mixer Type			
	Y-Mixer	T-Mixer	External Injection	Internal Injection
Number of elements	492,000	480,000	514,000	762,000
Maximum wall y+ value	2.8783	1.7129	1.0974	0.2505

2.2 Model Setup

To simulate proper operating conditions, several mathematical models readily available in the ANSYS FLUENT software were activated and utilized, i.e., continuity and momentum equations (Navier-Stokes equation) in the x, y, and z directions. The realizable k-ε model was used as the mathematical model to simulate the turbulence flow. Additionally, the non-equilibrium wall function was used to estimate parameters in the near-wall region. The selected mathematical models were solved using the second-order upwind scheme. The error tolerance was set at 10^{-6} to produce a more accurate solution.

2.2.1 Governing equations

The transfer of fluid or gas can be described by the continuity equation. The term "conservation of mass" often refers to the continuity equation. Since the total mass of the fluids entering through the two inlets and the total mass of the fluids exiting through the mixing out are equal, this equation is used to demonstrate mass conservation. The equation describes a fluid's ability to conserve mass while moving. The mass conservation equation applicable for both compressible as well as incompressible fluid flow is expressed by Andersson *et al.*, [18] as follows.

$$\frac{\partial \rho}{\partial t} + \nabla \cdot (\rho \vec{v}) = S_m \tag{1}$$

In the Eq. (1), ρ is the density of the fluid, v is the fluid velocity, and S_m is the mass transferred to the continuous phase from the dispersed second phase (e.g., due to vaporization of liquid) or other user-defined sources.

The momentum equation, often referred to as the Navier-Stokes equation, is used to calculate the resultant force imposed on the boundaries or walls of a flow passage as the flow changes direction, velocity, or both. On an inertial (non-accelerating) reference frame, the conservation of momentum is described by Eq. (2) as follows.

$$\frac{\partial \rho}{\partial t}(\rho \vec{v}) + \nabla \cdot (\rho \vec{v} \vec{v}) = -\nabla \mathrm{p} + \nabla \cdot (\bar{\bar{\tau}}) + \rho \vec{g} + \vec{F} \tag{2}$$

In the Eq. (2), p is the pressure of the fluid, τ is the stress tensor by the fluid, $\vec{g}$ is gravitational acceleration, and $\vec{F}$ is the force vector. The k-ε realizable model is based upon the transport equations for turbulence kinetic energy (k) and its dissipation rate (ε). For the model to be considered "realizable", it must adhere to specific mathematical constraints on the Reynolds stresses, which are in accordance with the physics of turbulent flows. Turbulent viscosity has a different formulation in the realizable k-ε model. A more precise equation for the transport of the mean-square vorticity fluctuation was used to develop a modified transport equation for the dissipation rate. The k and ε in the realizable k-ε model were modeled as the transport equation depicted in Eqs. (3) and (4).

$$\frac{\partial}{\partial t}(\rho k) + \frac{\partial}{\partial x_j}\left(\rho k \mathrm{u}_j\right) = \frac{\partial}{\partial x_j}\left[\left(\mu + \frac{\mu_t}{\sigma_k}\right)\frac{\partial k}{\partial x_j}\right] + G_k + G_b - \rho\varepsilon - Y_M + S_k \tag{3}$$

$$\frac{\partial}{\partial t}(\rho \varepsilon) + \frac{\partial}{\partial x_j}\left(\rho \varepsilon \mathrm{u}_j\right) = \frac{\partial}{\partial x_j}\left[\left(\mu + \frac{\mu_t}{\sigma_l}\right)\frac{\partial k}{\partial x_\varepsilon}\right] + \rho C_1 S \varepsilon - \rho C_2 \frac{\varepsilon^2}{k + \sqrt{\nu\varepsilon}} \tag{4}$$

where

$$C_1 = max\left[0.43, \frac{\eta}{\eta + 5}\right] \tag{5}$$

$$\eta = S\frac{k}{\varepsilon} \tag{6}$$

$$S = \sqrt{2 S_{ij} S_{ij}} \tag{7}$$

In the Eq. (3)-(7), *k* is the turbulent kinetic energy, u_j is the velocity magnitude on the y-axis, μ is the dynamic viscosity, μ_t is the eddy viscosity, σ is turbulent Prandtl numbers, G_k is the generation of turbulence kinetic energy due to mean velocity gradients, G_k is the generation of turbulence kinetic energy due to buoyancy, Y_M is the contribution of fluctuating dilatation in compressible turbulence to overall dissipation rate, ε is the dissipation rate, $C_{1\varepsilon}$; C_2 are constants, ν is the kinematic viscosity, η is the effectiveness factor, S is the modulus of mean rate-of-strain tensor, and S_{ij} is the mean rate-of-strain tensor.

2.2.2 Boundary conditions

Each inline mixer has two inlets and one outlet. Water entered the mixer through two inlets, namely the main inlet and the branch inlet, with varying average velocities, as shown in Table 2. The temperature of all inlets was set to 28°C (301,15 K). For the result to be more realistic, a user-defined function (UDF) was employed to imitate a fully-developed flow on the pipe's entrance. The UDF was derived based on Eq. (8) and (9) formulated by Bird *et al*., [19].

$$\frac{\bar{v}_z}{\bar{v}_{z,max}} \approx \left(1 - \frac{r}{R}\right)^{1/7} \tag{8}$$

$$\frac{\langle \bar{v}_z \rangle}{\bar{v}_{z,max}} \approx \frac{4}{5} \tag{9}$$

Table 2
Inlet boundary conditions

Mixer Type	Reynolds Number	Velocity or $\langle \bar{v}_z \rangle$, m/s		Mass Flow, kg/s	
		Pipe 1 (Main)	Pipe 2 (Branch)	Pipe 1 (Main)	Pipe 2 (Branch)
Spatial-Shaped Mixers	5,000	0.0494	0.0494	0.1000	0.1000
	10,000	0.0989	0.0989	0.2001	0.2001
	30,000	0.2967	0.2967	0.6003	0.6003
	50,000	0.4945	0.4945	1.0004	1.0004
	100,000	0.9890	0.9890	2.0009	2.0009
	200,000	1.9780	1.9780	4.0018	4.0018
Injection Mixers	5,000	0.0899	0.5754	0.1819	0.0182
	10,000	0.1798	1.1508	0.3638	0.0364
	30,000	0.5394	3.4525	1.0914	0.1091
	50,000	0.8991	5.7541	1.8190	0.1819
	100,000	1.7982	11.5082	3.6380	0.3638
	200,000	3.5963	23.0164	7.2760	0.7276

In the above equations, $\bar{v}_z$ is the time-smoothed velocity on the *z*-axis, r is the radial position, and R is the radius of the plane. In three-dimensional space, the time-smoothed velocity has to consider the *x* and *y*-axis positions. The outlet condition was designated as a pressure outlet with a pressure of 1 atm, while the boundary conditions on the wall was set as a no-slip condition.

2.3 Model Validation

A model validation process is necessary to ensure that the model used in the simulation is suitable to solve related phenomena. Model validation was carried out by comparing simulation results with experimental data presented by Walker *et al.,* [9]. The experimental campaign was carried out in T-type inline mixer with wire-mesh sensors to monitor the velocity magnitude. Mixing characteristics at several Reynolds number levels were analyzed, and the comparison with the current work was conducted at Reynolds number 50,000.

3. Results

3.1 Model Validation

The simulation work of this study was validated against experimental work carried out by Walker *et al*., [9]. In this study, the working fluid is water supplied from two different pipe sources i.e., main

and branch pipes, which then merged at T-type inline mixer before discharged through the outlet. Conductivity distributions at downstream of T-type mixer was monitored using wire-mesh sensors with a grid of 16x16 measuring points.

A set of wire-mesh sensors (WMS) with a grid of 16 × 16 measuring points was used to record conductivity distributions downstream of the T-junction. Based on the conductivity measurements, the velocity distribution at each measurement point was able to be recalculated. The velocity calculation was based on a double-sensor configuration which considered the time-of-flight measurements of fluid between two sensors. An improvement of the aforementioned method was conducted by allowing the correlation calculation for one point in the first sensor plane to be consistently computed for all nine neighboring points in the second sensor. Thus, the highest correlation coefficient at a certain point was used to determine the time-of-flight.

Based on the comparison between experimental and simulation results in Figure 4, it can be concluded that the current model can predict the velocity distribution inside the experimental pipe reasonably well. The comparison was conducted at two different positions, namely at approximately 6 inches and 12.2 inches from the mixing point or at x/D =3.0 and x/D = 6.1. It can be seen from Figure 4a or at 6 inches from the junction measurement point that higher velocity is obtained at the opposite side of branch pipe location which provided a similar profile as observed in the experimental work. Meanwhile, the symmetrical profile was identified at the most downstream measurement, namely at x/D = 6.1, as depicted in Figure 4(b). Slight discrepancies were obtained in several spot, in Figure 4, in term of absolute velocity value. This can be addressed due to the low resolution of the wire mesh sensor that was utilized in the experimental campaign. In general, this comparison shows the accuracy of the current developed model to be used in predicting hydrodynamic characteristics in the T-junction geometry and other mixer types.

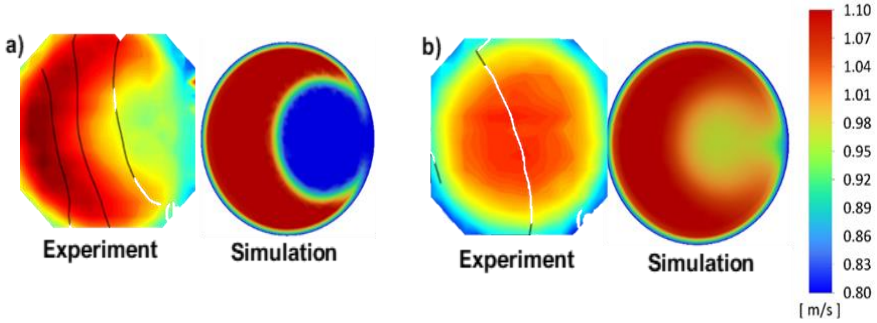

Fig. 4. Comparison between the experimental and simulation velocity contour at Re number 50,000, (a) at x/D = 3.0, and (b) x/D=6.1

3.2 Velocity Profile Development

The validated model was used further to simulate hydrodynamic conditions in different mixer types at various Reynolds numbers. A user-defined function (UDF) for the inlet boundary condition was utilized to maintain a fully-developed velocity condition starting from the pipe inlet. The axial velocity profile at several locations from the inlet is depicted in Figure 5, and it can be concluded that a fully-developed region has been reached before the mixing point at the internal injection-type mixer. This is also consistent in different mixer types. The utilization of fully-developed UDF at inlet boundaries is beneficial in reducing the length of the upstream simulated pipe. Otherwise, a significantly longer pipe is needed to ensure that a fully-developed region has been achieved before

the mixing position. Consequently, more computational mesh is needed in order to increase computational efficiency.

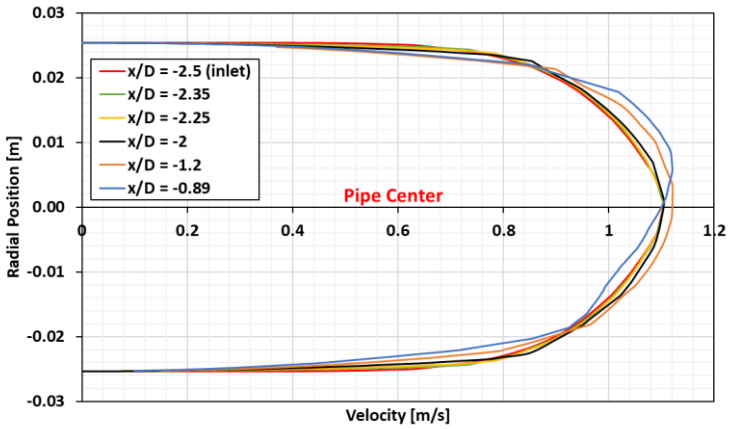

Fig. 5. Velocity profile close to inlet in Internal Injection mixer at Re = 50,000 (mixing point located at x/D = 0)

Figure 6 depicts the velocity profile at different mixer types for a particular Reynolds number, i.e., 50,000. Based on the velocity contour in Figure 6, information related to hydrodynamic regions can be exerted. It can be seen that different mixers provide different hydrodynamic region lengths. The Y-mixer type provides the shortest length to reach a fully-developed region based on visual assessment, while injection-type mixers need a significantly longer pipe length to reach a fully-developed region. Since similar components were used in this study for both inlet streams at various mixer types, the mixing performance observation was challenging.

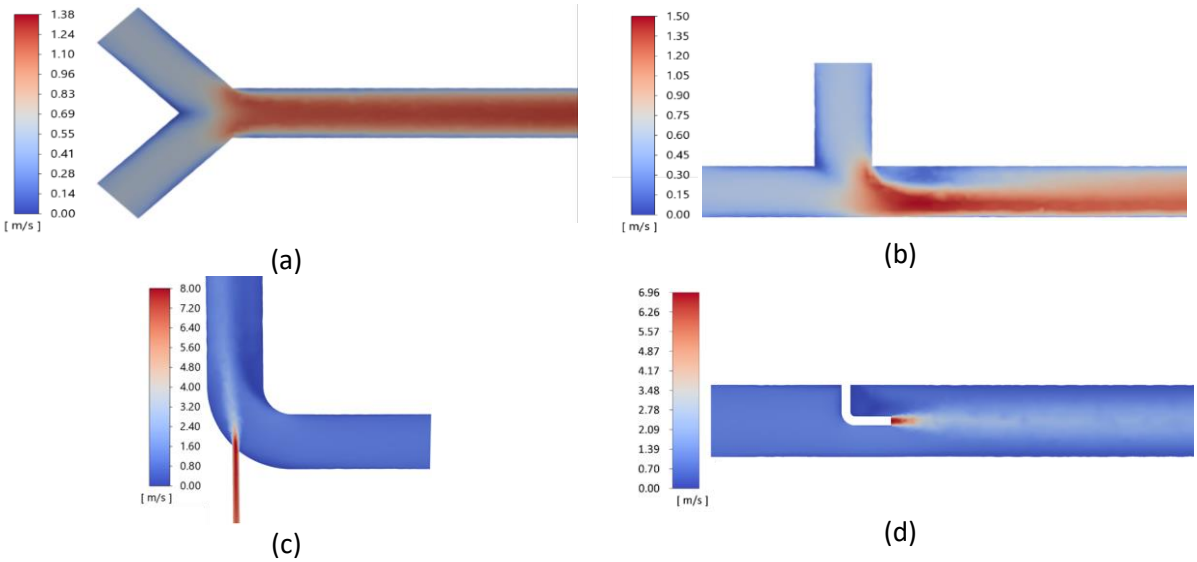

Fig. 6. Velocity contour plot in different mixer type for Reynold number 50,000 a) Y-Mixer, b) T-Mixer, c) External Injection (Elbow) Mixer, and d) Internal Injection Mixer

Velocity profile development at the pipe center for various mixer types is presented in Figure 8. The center pipe region is found to be the latest region that achieved a stable velocity value. Therefore, the utilization of pipe center observations is considered to be accurate in determining hydrodynamic region length. Figure 8 shows that lower Reynolds number conditions provide shorter distances to achieve final stable velocity. This is consistent in all mixer types examined in this study.

Overall, Y-type and T-type mixers require shorter distances to achieve a fully-developed region compared to the injection mixer type in various Reynolds numbers, as presented in Figure 8.

On average, the T-type mixers require approximately 1.5 times longer pipe to reach a fully-developed region compared to the Y-type mixers. This significant difference can be attributed to the flow channeling toward the opposite side of the branch pipe after the T-junction. The unsymmetric flow structure creates instability, producing a longer distance to develop a constant velocity profile. The vortex-like structure was also found just after the junction in the pipe region close to the branch pipe, as depicted in Figure 7. This vortex structure created a backflow which was also observed experimentally in previous work by Walker *et al.,* [9]. Better vortices resolution might be further observed using a more advanced turbulence model such as large eddy simulation (LES) [11].

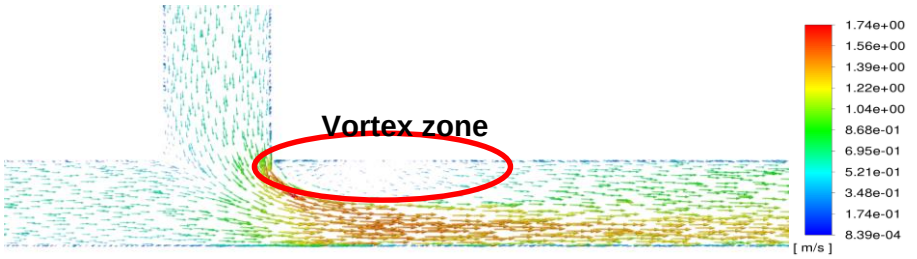

Fig. 7. Velocity vector plot in T-Mixer for Reynold number 50,000

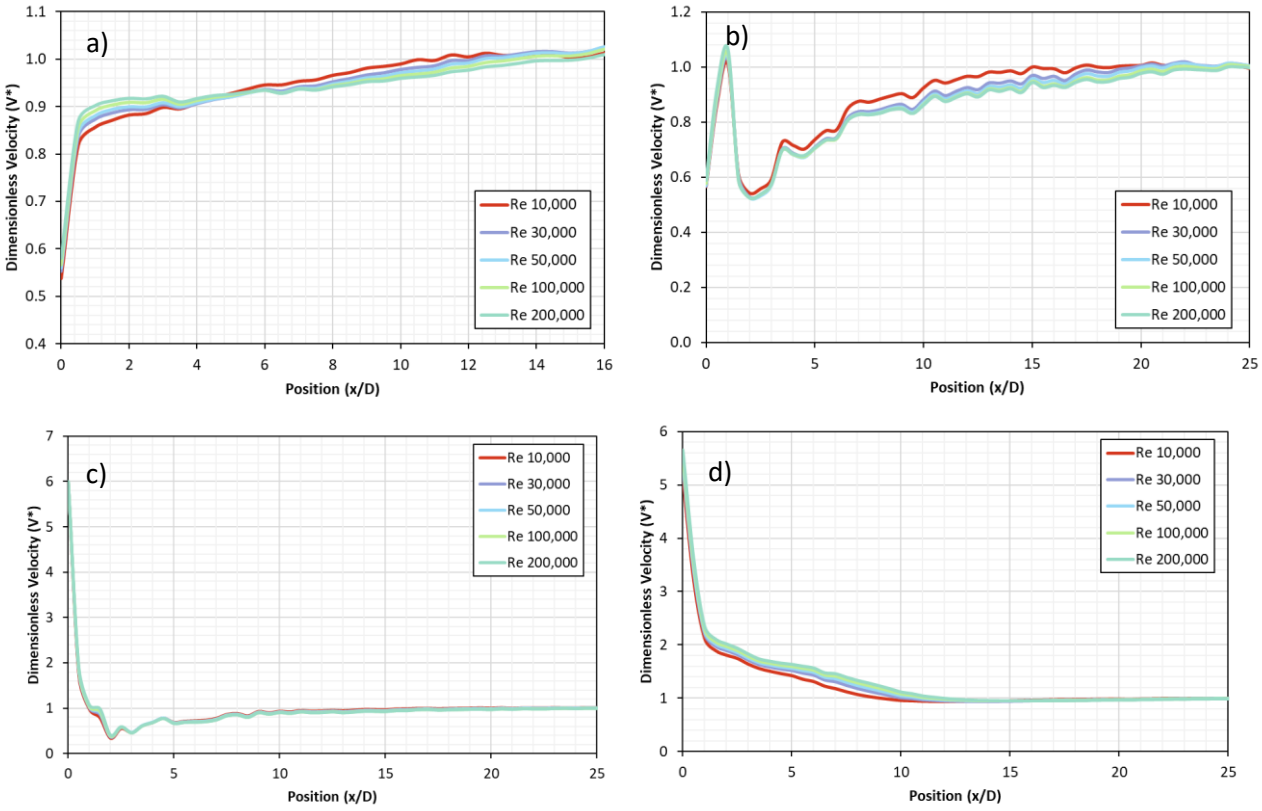

Fig. 8. Velocity profile at pipe center at different pipe length for a) Y-Mixer, b) T-Mixer, c) External Injection (Elbow) Mixer, and d) Internal Injection Mixer

An insignificant difference in hydrodynamic region length for the injection mixer type was identified based on CFD simulation results in Figure 6. It was observed that approximately 1.1 times longer pipe was needed to reach the fully-developed region for internal injection compared to the elbow injection mixer type. This slightly longer length in the internal injection mixer type can be

attributed to flow separation that happened after the main flow hit the injector pipe. This flow separation was found to create slight instability in the downstream mixed flow; thus longer distance was required to reach a fully-developed region.

3.3 Wall Stress Distribution

Another essential parameter to evaluate the hydrodynamic condition in different inline mixer types is stress analysis around the wall region. This parameter is crucial in predicting material fatigue and abrasion. These phenomena could lead to pipe cracking and leaking, especially while handling corrosive fluid in a high-pressure system. Figure 9 shows several potential hot spots for the material failure of four types of inline mixers that were analyzed in the study.

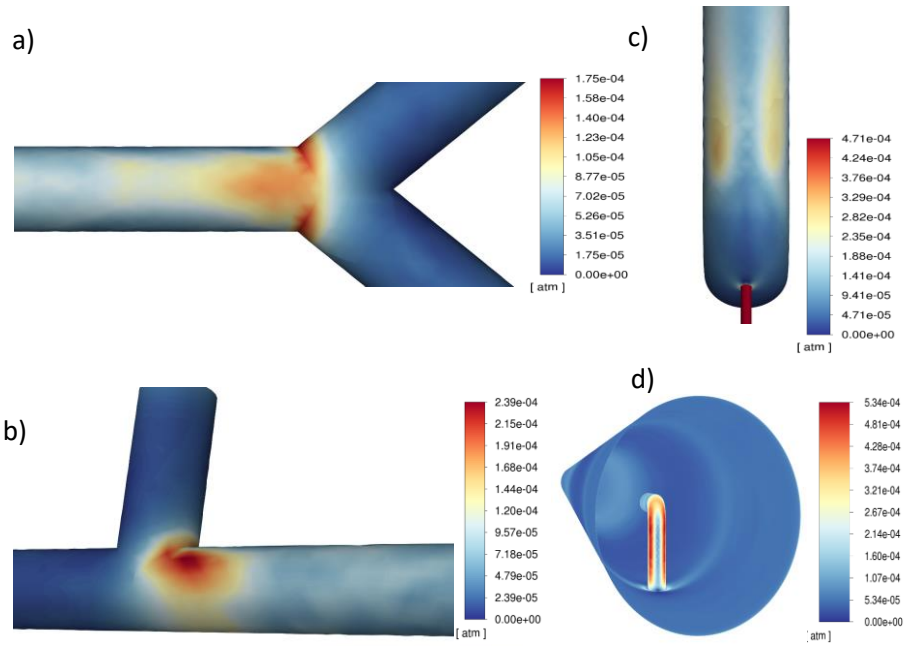

Fig. 9. Wall shear stress contour plot in different mixer types for Reynold number 50,000 a) Y-Mixer, b) T-Mixer, c) External Injection (Elbow) Mixer, and d) Internal Injection Mixer

Based on Figure 9, it can be determined that the maximum wall shear stress for Y and T-type mixers is located at the mixer joint. For the same Reynolds number, the maximum wall shear stress in the T-type mixer is approximately 1.4 times larger than the maximum wall shear stress in the Y-type mixer. This can be attributed to flow acceleration close to the T-type mixer junction, which directed the branch stream toward the wall region. The vortex located at the center pipe region, as indicated in Figure 7, enhanced this flow localization toward the wall area. Meanwhile, significantly lower wall shear stress was identified at the wall area where flow separation occurred.

Wall shear stress for the elbow mixer type is presented in Figure 9(c). The maximum wall shear stress after two streams mixing in the elbow mixer type was observed at the far side of the original main flow. This can be attributed to main flow impingement as a result of flow direction change. The distribution of maximum wall shear stress in elbow flow was found to be different with and without mixing from branch pipe. In a previous study by Ajmal *et al.*, [6] maximum wall shear stress was identified at the inside side of the elbow or intrados. Due to the injection of secondary flow from the branch pipe, the wall shear stress hotspot was changed toward the extrados area.

About twice as large maximum wall shear stress was identified in the internal injection mixer type compared to the elbow type mixer. The maximum wall shear stress was not located in the main pipe stream but on the outer side of the injection pipe, as presented in Figure 9(d), and primary flow impingement caused this high shear stress at the injection pipe. For the same Reynolds number, it was found that the internal injection mixer generated the highest wall shear stress compared to the other inline mixer types.

3.4 Correlation of Hydrodynamic Region Length to Reynolds Number

The hydrodynamic region length in different Reynolds numbers has been simulated in various commercial inline mixers. The absolute value of hydrodynamic region lengths can be estimated directly from CFD simulation. In this study, the location where no velocity fluctuation was identified and utilized to determine the boundary of the hydrodynamic and fully-developed regions. The final absolute values of the fluctuating velocity regions are summarized in Table 3 for different mixer types in various Reynolds number range (5,000 to 200,000).

Table 3
Hydrodynamic region length of various inline mixers at various Reynolds number

Reynolds Number	Hydrodynamic Region Length Position [x/D]			
	Y-Mixer	T-Mixer	External Injection	Internal Injection
5,000	9.00	12.00	14.00	17.50
10,000	10.00	15.00	16.00	19.50
30,000	11.00	17.50	18.50	21.50
50,000	11.50	19.50	20.50	22.00
100,000	12.50	20.00	21.50	23.50
200,000	13.00	21.50	23.00	24.50

Based on Table 3 and Figure 9, higher Reynolds numbers provide longer hydrodynamic regions in all mixer types. This can be attributed to higher Reynolds numbers which create more intensive turbulence, which could subsequently cause longer distances to create stability in a fluid flow system. The results of this study are found to be similar to the results of a study carried out by Sinnot *et al.,* [3]. The study by Sinnot *et al.,* [3] identified approximately 10 -20 times diameter to achieve a stable region in a T-type inline mixer. This study found that a minimum length of 12 times the diameter is needed to reach the fully-developed region in the T-type mixer, as presented in Table 3. A formulation that correlates hydrodynamic region length to Reynolds number can be generated based on data presented in Table 3. Non-linear regressions were conducted to formulate a logarithmic correlation of hydrodynamic region length as a function of the Reynolds number. The final equation for each mixer type is presented in Table 4. The model formulation of hydrodynamic lengths is proven to be accurate based on the comparison to CFD simulation results, as presented in Figure 10.

Table 4
Equation of hydrodynamic region length (L_e) as a function of Reynolds number

Mixer Type	Equation	R-Squared
Y-Mixer	L_e = 1.0806 ln (Re) - 0.1035	0.9933
T-Mixer	L_e = 2.5063 ln (Re) - 8.5555	0.9657
External Injection (Elbow)	L_e = 2.4563 ln (Re) - 6.701	0.9907
Internal Injection	L_e = 1.8443 ln (Re) + 2.1823	0.9874

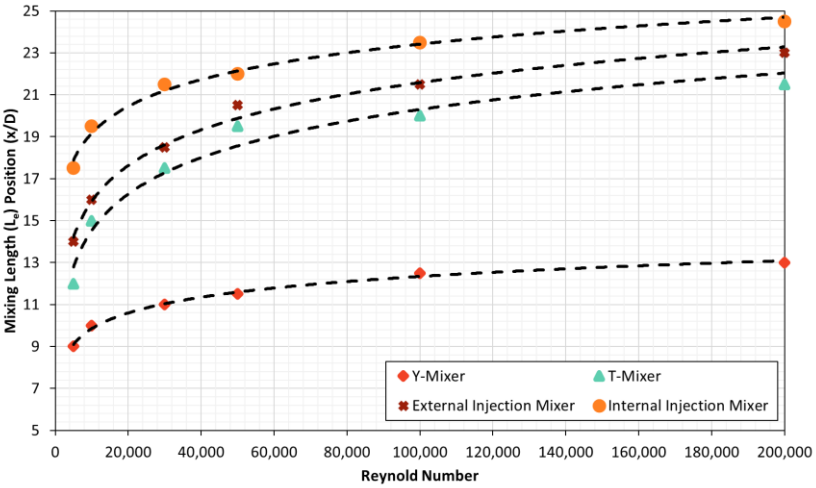

Fig. 10. Comparison of hydrodynamic region length from CFD simulation and model formulation in Table 4

4. Conclusions

This study presents an evaluation of hydrodynamic region characteristics in several inline mixer types using computational fluid dynamics analysis. Four different commercial inline mixer types were evaluated, namely Y-type, T-type, elbow type, and internal injection mixer type. The analysis was conducted using commercial CFD software, i.e., ANSYS Fluent 2022R1, which includes geometry modeling, mesh generation, and simulation setups. To ensure simulation accuracy, a mesh independence test was conducted for all mixer types. Velocity user-defined function at inlet boundary conditions was defined to maintain a fully-developed velocity profile starting from the stream inlet. The hydrodynamic characteristics evaluation was performed for several Reynolds number conditions, from 5,000 to 200,000.

Model validation was also performed to determine model accuracy. A high degree of agreement between the CFD results and previous experimental results is proven by the contour plots' similarity in the T-pipe type system. Among four different inline mixers, the Y-type mixer type is found to provide the shortest distance to reach a fully-developed region for the same Reynolds number. Meanwhile, the internal injection type is identified to have the longest hydrodynamic region length.

Based on the CFD results, the distribution of wall shear stress in different inline mixer types was also evaluated. The highest wall stress is identified in the injection inline mixer type, i.e., at the outer side wall of the injection pipe. Meanwhile, the mixer joint in the T-type and Y-type mixers are found to have a wall shear stress hotspot. The maximum wall shear stress in the elbow type mixer is observed to be located around the extrados area.

Correlations of hydrodynamic region length to Reynolds number were generated for the four different inlet mixer types. Logarithmic correlation can accurately represent the correlation between hydrodynamic region length and Reynolds number for all mixer types with an average R-squared of approximately 0.98. This correlation is extremely important and can be further used as a basis for inline mixer selection and detail engineering design in the industrial sector.

Acknowledgment

This research was funded by a grant from Chemical Engineering Department, Universitas Gadjah Mada (Grant number: 1580103/UN1.FTK/SK/HK/2022).

References

[1] Uhl, Vincent, ed. *Mixing V1: Theory and practice*. Elsevier, 2012.
[2] Sroka, L. M., and L. J. Forney. "Fluid mixing with a pipeline tee: theory and experiment." *AIChE journal* 35, no. 3 (1989): 406-414. https://doi.org/10.1002/aic.690350308
[3] Sinnott, Raymond K., John Metcalfe Coulson, and John Francis Richardson. *Chemical engineering design*. Vol. 6, no. 4. Oxford: Elsevier Butterworth-Heinemann, 2005.
[4] Cengel, Yunus, and John Cimbala. *Ebook: Fluid mechanics fundamentals and applications*. McGraw Hill, 2006.
[5] Sigalotti, Leonardo Di G., Carlos E. Alvarado-Rodríguez, Jaime Klapp, and José M. Cela. "Smoothed particle hydrodynamics simulations of water flow in a 90 pipe bend." *Water* 13, no. 8 (2021): 1081. https://doi.org/10.3390/w13081081
[6] Ajmal, T. S., Shashi Bhushan Arya, and K. Rajendra Udupa. "Effect of hydrodynamics on the flow accelerated corrosion (FAC) and electrochemical impedance behavior of line pipe steel for petroleum industry." *International Journal of Pressure Vessels and Piping* 174 (2019): 42-53. https://doi.org/10.1016/j.ijpvp.2019.05.013
[7] Nan, Zezhao, Xianqiao Zhao, Yaru Li, Keyuan Zhang, and Naihua Wang. "Thermal mixing in T-junctions with different incident angle of branch pipe." *International Journal of Heat and Mass Transfer* 181 (2021): 121834. https://doi.org/10.1016/j.ijheatmasstransfer.2021.121834
[8] Nan, Zezhao, Mingzhou Gu, Yaru Li, Keyuan Zhang, and Naihua Wang. "Effects of the incident angle of branch pipe on the thermal mixing of impinging jets in T-junctions." *International Journal of Heat and Mass Transfer* 185 (2022): 122433. https://doi.org/10.1016/j.ijheatmasstransfer.2021.122433
[9] Walker, Christopher, Marco Simiano, Robert Zboray, and H-M. Prasser. "Investigations on mixing phenomena in single-phase flow in a T-junction geometry." *Nuclear Engineering and Design* 239, no. 1 (2009): 116-126. https://doi.org/10.1016/j.nucengdes.2008.09.003
[10] Austin, R. G., B. van Bloemen Waanders, S. McKenna, and C. Y. Choi. "Mixing at cross junctions in water distribution systems. II: Experimental study." *Journal of Water Resources Planning and Management* 134, no. 3 (2008): 295-302. https://doi.org/10.1061/(ASCE)0733-9496(2008)134:3(295)
[11] Baranova, Tatyana A., Yulia V. Zhukova, Andrei D. Chorny, Artem Skrypnik, and Igor A. Popov. "Non-Isothermal Vortex Flow in the T-Junction Pipe." *Energies* 14, no. 21 (2021): 7002. https://doi.org/10.3390/en14217002
[12] Romero-Gomez, P., C. K. Ho, and C. Y. Choi. "Mixing at cross junctions in water distribution systems. I: Numerical study." *Journal of Water Resources Planning and Management* 134, no. 3 (2008): 285-294. https://doi.org/10.1061/(ASCE)0733-9496(2008)134:3(285)
[13] Nuruzzaman, Md, William Pao, Hamdan Ya, Md Ragibul Islam, Mohammad Ayub Adar, and Faheem Ejaz. "Simulation analysis of thermal mixing characteristics of fluids flowing through a converging T-junction." *CFD Letters* 13, no. 9 (2021): 28-41. https://doi.org/10.37934/cfdl.13.9.2841
[14] Huang, Kexin, Bo Su, Tong Li, Hanbing Ke, Mei Lin, and Qiuwang Wang. "Numerical simulation of the mixing behaviour of hot and cold fluids in the rectangular T-junction with/without an impeller." *Applied thermal engineering* 204 (2022): 117942. https://doi.org/10.1016/j.applthermaleng.2021.117942
[15] Ouregani, Najmeh J., Hossein Abdi, and Vladimir I. Melikhov. "OpenFOAM modeling of thermal mixing in a T-junction geometry using RANS and LES models." In *2022 4th International Youth Conference on Radio Electronics, Electrical and Power Engineering (REEPE)*, pp. 1-6. IEEE, 2022. https://doi.org/10.1109/REEPE53907.2022.9731494
[16] Isaev, Alexander, Jonina Felbinger, and Eckart Laurien. "Numerical investigation on similarity of isothermal and thermal flow mixing in a horizontal T-junction configuration." *International Journal of Heat and Fluid Flow* 92 (2021): 108861. https://doi.org/10.1016/j.ijheatfluidflow.2021.108861
[17] Lampunio, Lisa, Yu Duan, and Matthew D. Eaton. "The effect of inlet flow conditions upon thermal mixing and conjugate heat transfer within the wall of a T-Junction." *Nuclear Engineering and Design* 385 (2021): 111484. https://doi.org/10.1016/j.nucengdes.2021.111484
[18] Andersson, Bengt, Ronnie Andersson, Love Håkansson, Mikael Mortensen, Rahman Sudiyo, and Berend Van Wachem. *Computational fluid dynamics for engineers*. Cambridge university press, 2011. https://doi.org/10.1017/CBO9781139093590
[19] R. B. Bird, W. E. Stewart, and E. N. Lightfoot, *Transport Phenomena*. Wiley, 2006.